Structural Monitoring and Maintenance, *Vol. 3, No. 3 (2016) 297-314*
DOI: http://dx.doi.org/10.12989/smm.2016.3.3.297

FE and ANN model of ECS to simulate the pipelines suffer from internal corrosion

Wael A. Altabey*[1,2]

[1]*International Institute for Urban Systems Engineering, Southeast University, Nanjing (210096), China*
[2]*Department of Mechanical Engineering, Faculty of Engineering, Alexandria University, Alexandria (21544), Egypt*

(Received February 9, 2016, Revised May 15, 2016, Accepted June 9, 2016)

Abstract. As the study of internal corrosion of pipeline need a large number of experiments as well as long time, so there is a need for new computational technique to expand the spectrum of the results and to save time. The present work represents a new non-destructive evaluation (NDE) technique for detecting the internal corrosion inside pipeline by evaluating the dielectric properties of steel pipe at room temperature by using electrical capacitance sensor (ECS), then predict the effect of pipeline environment temperature (θ) on the corrosion rates by designing an efficient artificial neural network (ANN) architecture. ECS consists of number of electrodes mounted on the outer surface of pipeline, the sensor shape, electrode configuration, and the number of electrodes that comprise three key elements of two dimensional capacitance sensors are illustrated. The variation in the dielectric signatures was employed to design electrical capacitance sensor (ECS) with high sensitivity to detect such defects. The rules of 24-electrode sensor parameters such as capacitance, capacitance change, and change rate of capacitance are discussed by ANSYS and MATLAB, which are combined to simulate sensor characteristic. A feed-forward neural network (FFNN) structure are applied, trained and tested to predict the finite element (FE) results of corrosion rates under room temperature, and then used the trained FFNN to predict corrosion rates at different temperature using MATLAB neural network toolbox. The FE results are in excellent agreement with an FFNN results, thus validating the accuracy and reliability of the proposed technique and leads to better understanding of the corrosion mechanism under different pipeline environmental temperature.

Keywords: Electrical Capacitance Sensor (ECS); internal corrosion detection; artificial neural; network (ANN)

1. Introduction

Pipelines play an extremely important role throughout the world as means of transporting gases and liquids over long distances from their sources to the ultimate consumers. Pipelines suffer from corrosion, cracking and other problems. Internal corrosion has been recognized for many years as one of the main deterioration mechanisms that may reduce the structural properties of transmission

*Corresponding author, Assistant Professor, E-mail: wael.altabey@gmail.com
[1] Current Affiliation
[2] Previous Affiliation

http://www.techno-press.org/?journal=smm&subpage=7 ISSN: 2288-6605 (Print), 2288-6613 (Online)

pipelines.

Therefore, the ability to detect such damages at an early stage is essential to assess the pipe integrity and long-term performance of these pipes. Various non-destructive evaluation (NDE) techniques have been studied to detect corrosion of metallic pipes such as x-ray, gamma-ray radiography, ultrasonic, thermography and eddy current (He 2015, Cole and Marney 2012), fiber optic distributed (Sinchenko 2013, Alwis *et al.* 2013, Dong *et al.* 2005a, b, Dong *et al.* 2007, Li *et al.* 2000).

The different NDE methods indicates several difficulties associated with their field application due to their requirements of heat or wave sources, and complicated data analyzers, also limited to cover the large area of detecting and the difficulties associated with interpretations of the results.

The objective of this study is to present a new practical technique for internal corrosion detection inside steel pipes by detecting the local variation of the dielectric properties of materials using an electrical capacitance sensor (ECS) and study the effect of pipeline environment temperature on the corrosion rates by using an efficient artificial neural network (ANN) architecture, with taking in to account the flow rate velocity and pressure effect.

2. Electrical Capacitance sensor (ECS)

ECS was first introduced in the 1980s by a group of researchers from the US Department of Energy Morgantown Energy Technology Center (METC), to measure fluidized bed system (Fasching and Smith 1988, Fasching and Smith 1991).

ECS is one of the most mature and promising methods, which measures the capacitance change of multi-electrode sensor due to the change of dielectric permittivity being imaged, and then reconstructs the cross-section images using the measured raw data with a suitable algorithm. It has the characteristics such as low cost, fast response, non-intrusive method, broad application, safety (Yang *et al.* 1995a, b, Li and Huang 2000). Electrical capacitance system includes sensor, capacitance measuring circuit and imaging computer is shown in Fig. 1. And ECS consists of insulating pipeline, measurement electrode, radial screen and earthed screen (Yang and York 1999). The measurement electrode is mounted symmetrically around the circumference of pipeline. Radial screen is fitted between the electrodes to cut the electro line external to the sensor pipeline and reduce the inter-electrode capacitance. The earthed screen surrounds the measurement electrodes to shield external electromagnetic noise. ECS converts the permittivity of inner media flow to inter-electrode capacitance, which is the ECS forward problem. Capacitance measuring circuit takes the capacitance data and transfers to imaging computer. Imaging computer reconstructs the distribution image with a suitable algorithm, which is called ECS inverse problem.

In most application, ECS electrode is mounted outside the pipeline which is called external electrode ECS (Yang 1997), so pipeline thickness is a very important parameter in ECS design. There are three factors which have great effect on ECS measurements, e.g. pipeline material, inner dielectric permittivity and the ratio of pipeline thickness and diameter (Jaworski and Bolton 2000, Daoye *et al.* 2009, Pei and Wang 2009, Al-Tabey 2010).

2.1 The ECS geometrical model

There are $N(N-1)/2$ electrodes pairs are installed on the outer wall symmetrically along the circumference of pipe, hence $N(N-1)/2$ independent capacitance measurements (where N is

the number of sensor electrodes). Fig. 2 is the partial from cross section of 24-electrode ECS, in which R_1 is inner pipeline radius; R_2 is outer pipeline radius; X is the pipe wall thickness; R_3 is earthed screen radius; and radial screen is connected to outer pipeline.

For the purpose of making the describe of pipeline corrosion (wall thickness) easier, the concept of radius-electrode ratio ρ ($\rho = R_1/R_2$) is put backward, which is the ratio of pipeline inner radius to electrode radius (i.e. pipeline outer radius). In ideal condition (No corrosion), pipeline wall thickness is $X = (R_2 - R_1)$, so ρ is equal to constant value of R_1/R_2. The larger radius-electrode ratio is the more serious the effect of pipeline corrosion becomes.

2.2 The ECS mathematical model

The system model for *ECS* is based on the electrostatic field theory, which can be used to find the potential distribution $\varphi(x, y)$ inside the ECS. By solving the Poisson's equation

$$\nabla.\varepsilon(x,y)\nabla.\varphi(x,y) = 0 \tag{1}$$

For the boundary condition imposed on the ECS head by the measurement system, the potential distribution $\varphi(x, y)$ can be found. The electric field vector $E(x, y)$ and the potential function $\varphi(x, y)$ are related as follows

$$E(x,y) = -\nabla\varphi(x,y) \tag{2}$$

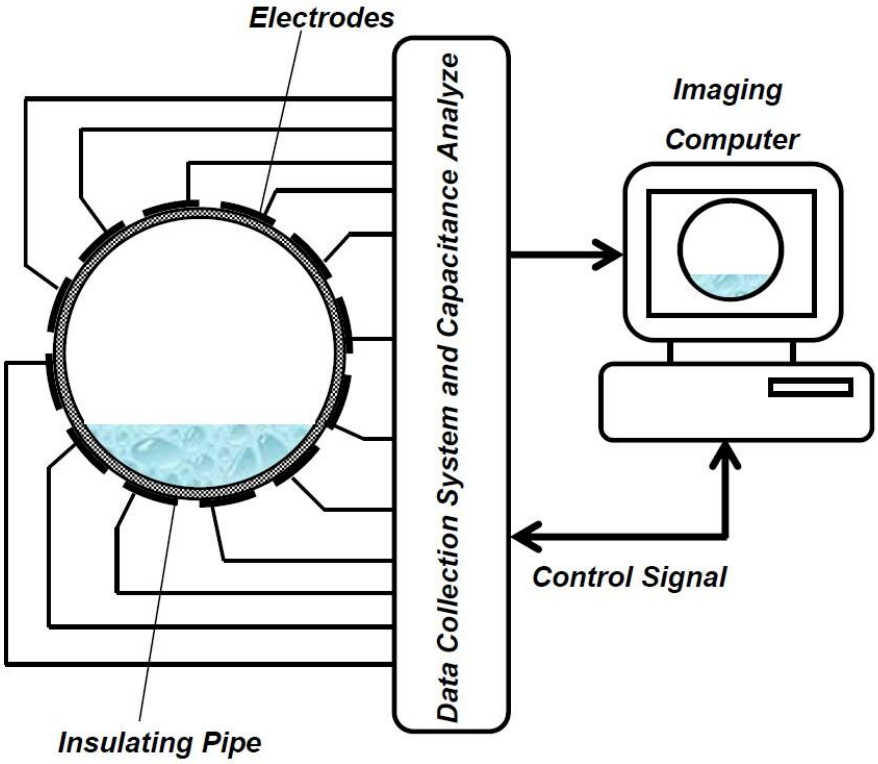

Fig. 1 Sketch of ECS system

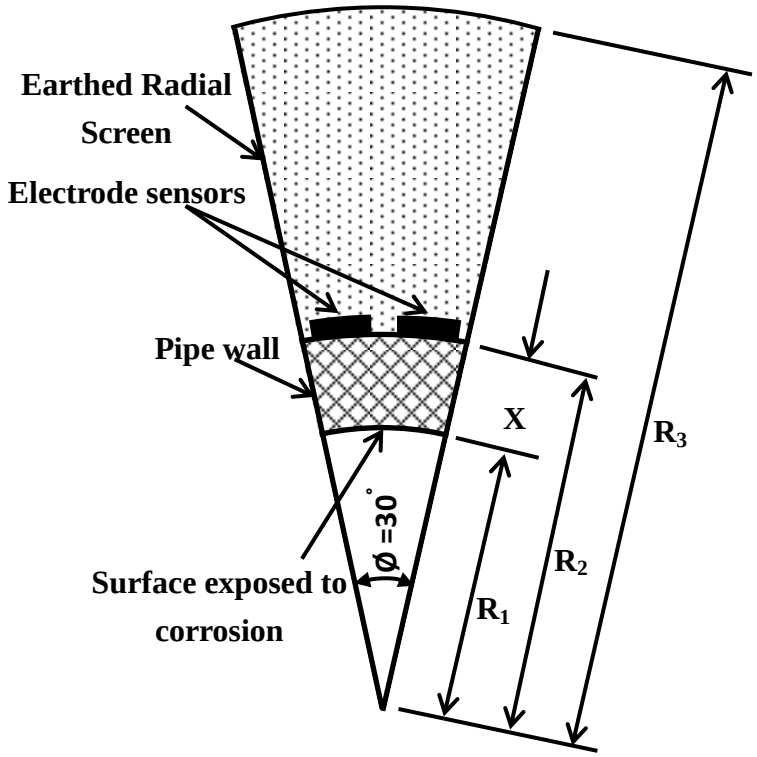

Fig. 2 The partial cross section sketch of ECS

The change on the electrodes, and hence the inter electrode capacitances can be found using the definition of the capacitance and Gauss's law based on the following surface integral

$$Q_{ij} = \oint_{S_j} (\varepsilon(x,y)\nabla\varphi(x,y).\hat{n})\, ds \tag{3}$$

Where: $\varphi(x,y)$ is potential distribution, $\varepsilon(x,y)$ is permittivity distribution, $E(x,y)$ is electric field vector, $\nabla.$ is divergence operator, ∇ is gradient operator, S_j is a surface enclosing electrode j, ds is an infinitesimal area on electrode j and $\hat{n}$ is the unit vector normal to S_j. Using these charge measurements Q_{ij}, the inter electrode capacitance C_{ij} can be compute using the definition of Eq. (4)

$$C_{ij} = \frac{Q_{ij}}{\Delta V_{ij}} \tag{4}$$

Where Q_{ij} is the charge induced on electrode (j) when electrode (i) is excited with a known potential, ΔV_{ij} is the potential difference between electrodes (i) and (j) $(\Delta V_{ij} = V_i - V_j)$.

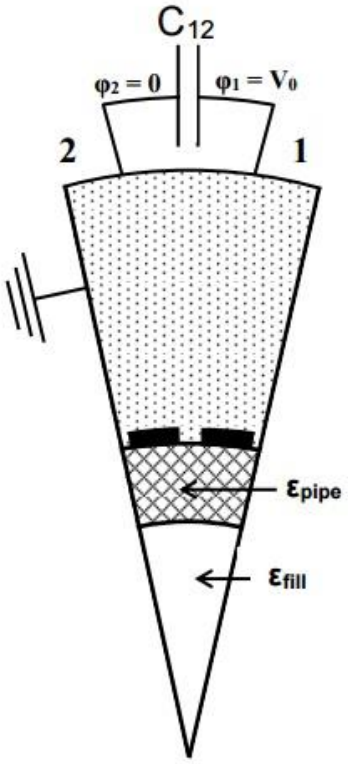

Fig. 3 Schematic representation of the measurement principle of an ECS

2.3 The ECS composition and working principle

When one electrode is excited, the other electrodes are kept at ground potential as shown in the Fig.3 and act as detector electrodes. When electrode No. 1 is excited with a potential, the change $Q_{1,j}$ is induced on the electrodes, $j = 2, \cdots\cdots, N$ can be measured. Next, electrode No. 2 is excited whereas, rest the electrodes are kept at ground potential, and the induced charges $Q_{23}, Q_{24}, \cdots, Q_{2N}$ are measured. The measurement protocol continues unit electrode N-1 is excited.

3. Finite Element Method (FEM) of ECS

In terms of Electrical Capacitance sensor (ECS), the forward problem is the problem of calculating the capacitance matrix C from a given set of sensor design parameters and a given cross-sectional permittivity distribution ε.

A 2D finite element simulation was selected for modeling the sensing system is based on forward model proposed by Xie *et al.* (1992).

By solving Eq. (1), the sensor potential distribution $\varphi(x, y)$ can be obtained. For the structure irregularity of sensor electrode pair and the in-homogeneity of dielectric distribution, Eq. (1)

doesn't exist analytical solution, but it can be worked out through FEM. When using FEM to solve problem, the continuous field should be converted to a discrete form, namely, the solution domain should be divided into finite elements. For the convenience of numerical simulation, the commercially available finite element software ANSYS (The Electrostatic Module in the Electromagnetic subsection of ANSYS 2014, Al-Tabey 2012) is used to build the 2D geometry model of sensor and divide the cross section domain into triangle elements, see Fig. 4. The partition results such as node coordinates, boundary condition and relation between elements and nodes are extracted to calculate potential distribution in MATLAB.

3.1 Boundary conditions

The potential boundary conditions were applied to the sensor-plate (electrodes). For one electrode, the boundary condition of electric potential ($V=V_0$) with 15V (V_0) was applied and another electrode was kept at ground (V=0) potential to simulate a 15V (RMS) potential gradient across the electrodes.

3.2 The geometric properties

Through simulation comparison of full pipeline of steel, we will get the distribution of electric sensitive potential and effect of pipeline corrosion on the sensitive field. The simulation settings of steel and water relative permittivity ε is 7.0, and 80, respectively and set number 24 electrode excitation electrodes, excitation voltage V_0 = 15 volts, the sensor physical specification shown in Table 1.

3.3 The field partition

According to finite element analysis, we will carry out imaging of regional triangulation, it is necessary to divided pixel pipe into triangular finite element, because many pipes are round under the circumstances of a smaller number of pixels, we can achieve higher accuracy to use the triangle mesh than rectangular grids, To improve the accuracy of mesh, we will take subdivision method two times imaging region is divided into 562 Elements. To improve the accuracy of mesh, we divided the meshed region again into 997 Elements; the map is as follows in Fig. 4.

Table 1 Sensor physical specification

ECS system	**Specification**
No. of electrodes	24
Guards between electrodes	1 mm
Inner/outer pipe diameter	49.3/65.2 mm
Earth Screen diameter	120 mm
Thickness of electrodes	1mm
Permittivity pipe wall	ε_{pipe} = 7 Fm^{-1}
Permittivity of Water	ε_{fill} = 80 Fm^{-1}
Permittivity of Air	ε_A = 1.0 Fm^{-1}
Excitation voltage	φ = 15 Volts

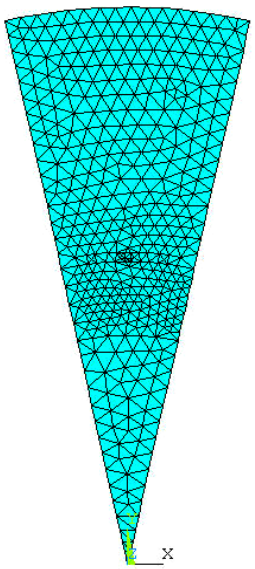

Fig. 4 Element map of finite element mesh

4. Results and discutions

4.1 Pipeline internal corrosion detection

The pipeline internal corrosion can occur when the pipe wall is exposed to water and contaminants in the filling fluid, such as chlorides. The nature and extent of the corrosion damage that may occur are functions of the concentration and particular combinations of these various corrosive constituents within the pipe, as well as of the operating conditions of the pipeline.

The pipeline internal corrosion is means decrease of the pipeline thickness at repeated time interval (i.e., the radius-electrode ratio ρ increases). This work is targeted for sensing the internal corrosion as it occurs to avoid the fraction problems. So in this section we will be discussed the effect of pipeline internal corrosion on ECS capacitance C_{ij} by decreasing of pipeline thickness X, or increasing of radius-electrode ratio ρ, and study the change in the electrode sensors capacitance.

The parameters of simulated ECS, which used in pipeline, include inner radius R_1, outer radius R_2, earthed screen radius R_3, solid permittivity ε_{pipe} and filling layer permittivity ε_{fill}. The outer radius is constant. The pipeline thickness $X = (R_2-R_1)$ is selected as X_1 = 7.95 mm, X_2 = 6.95 mm, X_3 = 5.95 mm, X_4 = 4.95 mm, X_5 = 3.95 mm, X_6= 2.95 mm and X_7 = 1.95 mm respectively, on the other hand the radius-electrode ratio $\rho = (1-(X/ R_2))$ equal to 0.76, 0.79, 0.82, 0.85, 0.88, 0.91, 0.94 respectively. The Simulations, and the node potential distribution of pipeline suffer from internal corrosion (pipe wall thickness decrease) at $\theta = 25℃$, when a constant current is injected between electrode 1 and 2 are illustrated in Fig. 5. The blue area represents the region of the pipe without potential i.e., $\varphi = 0$ but the colored areas represent the region of the pipe have the different potential (different node potential) i.e. the domain of electrode can be sensitive or detection domain.

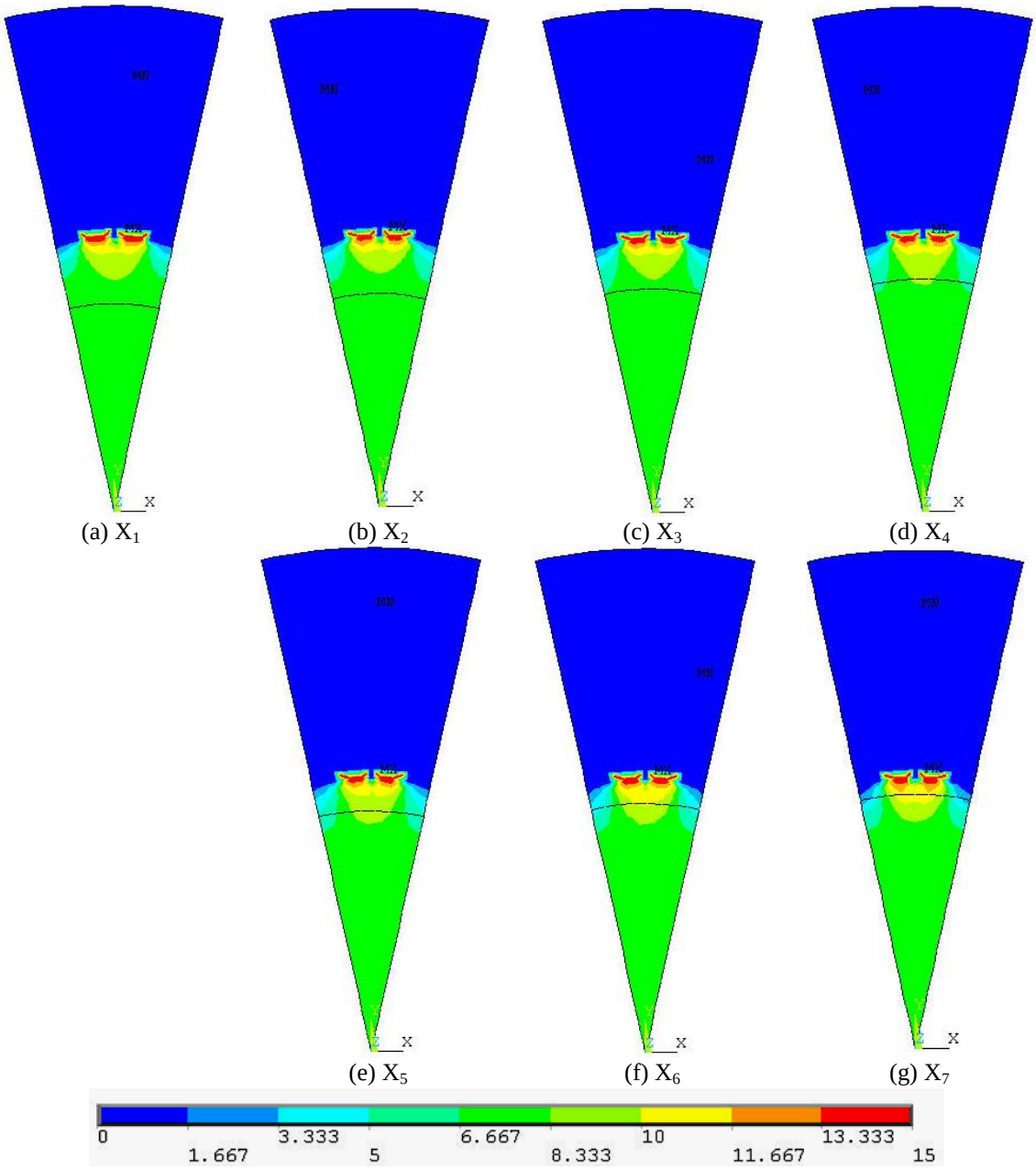

Fig. 5 The node potential distribution of pipe wall thickness at $\theta = 25℃$

4.2 Effect of pipeline corrosion on sensor capacitance

The effect of the pipeline internal corrosion on Capacitance change in Pico Farad (10^{-12}Farad) is calculated, and investigated. Because of symmetry, 24-electrode sensor has 12

typical structures of inter-electrode pair; hence only 12 inter electrode pairs ($C_{1\text{-}2}$, $C_{1\text{-}3}$, $C_{1\text{-}4}$, $C_{1\text{-}5}$, $C_{1\text{-}6}$, $C_{1\text{-}7}$, $C_{1\text{-}8}$, $C_{1\text{-}9}$, $C_{1\text{-}10}$, $C_{1\text{-}11}$, $C_{1\text{-}12}$ and $C_{1\text{-}13}$) are listed, as showing in Fig. 6.

The tendency curve of capacitance change against X is shown in Fig. 6. In adjacent electrode pair, capacitance change increases monotonously with the increase of X or decrease ρ, and turns to decrease with the increase of X. However, there exist maximum points in non-adjacent electrode pairs, and all the maximum values are at the same position where X= 6.95 mm, ρ = 0.79. So sensor with this ρ is more suitable to capacitance measurement.

Using the exponential formula (5) to fit the FE results of capacitance change have proved its suitability by giving acceptable values for the correlation factor (C.F) are very near to unity. The values of four constants (a_{ij}), (b_{ij}), (k_{ij}) and (h_{ij}) at $\theta = 25℃$ are displayed in Table 3.

$$C_{ij} = a_{ij}e^{b_{ij}X} + k_{ij}e^{h_{ij}X} \tag{5}$$

5. Artificial neural network (ANN) modeling

Artificial neural network (ANN) is an attractive inductive approach for modeling non-linear and complex systems without explicit physical representation and thus provides an alternative approach for modeling hydrologic systems. Artificial neural network was first developed in the 1940s. Generally speaking, ANNs are information processing systems. In recent decades, considerable interest has been raised over their practical applications. Training of artificial neural network enables the system to capture the complex and non-linear relationships that are not easily analyzed by using conventional methods such as linear and multiple regression methods and the network is built directly from experimental or numerical data by its self-organizing capabilities. Based on the different applications, various types of neural network with various algorithms have been employed to solve the different problems. In this work will be using the preferred ANN structures to predict the ECS capacitance change of presented numerical conditions.

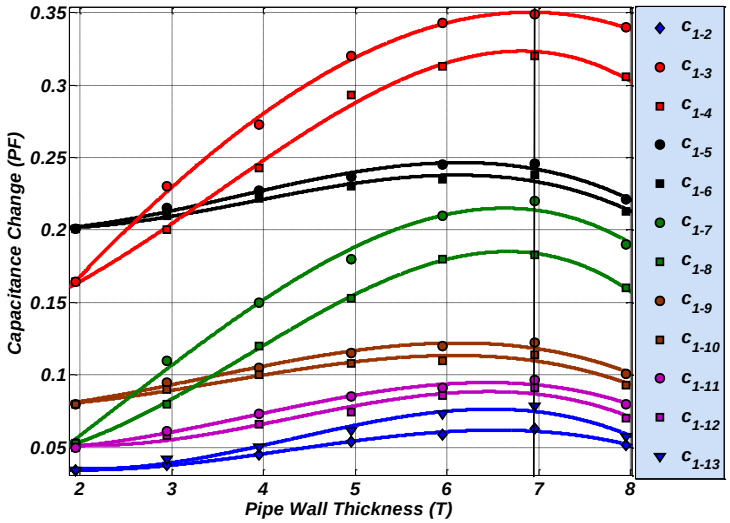

Fig. 6 Effect of Pipeline Corrosion on Capacitance change at $\theta = 25℃$

5.1 ANN configuration

Since the ANN configuration has a great influence on the predictive quality, various arrangements have been considered in previous work. It is necessary to define a simple code to describe the ANN configuration, as follows

$$\{N_{in}\ [N_{h1}\ N_{h2}]_e\ N_{out}\} \tag{6}$$

Where N_{in} and N_{out} are the element numbers of input and output parameters, respectively, and e is the number of hidden layers. N_{h1} and N_{h2} are numbers of neurons in each hidden layer, respectively. For example, $\{7\ [21]_1 1\}$ means a one hidden layer ANN with seven input and one output parameters, with the hidden layer containing 21 elements (neurons); $\{9\ [15\ 10]_2 1\}$ denotes a nine input and one output ANN, with 15 and 10 neurons, respectively, in three hidden layers.

The powerful function of an ANN is due to the neurons within the hidden layers, as well as to the related interconnections. Networks are also sensitive to the number of neurons in their hidden layers. It is believed that an ANN can represent any reasonable relationship between input and output if the hidden layers have enough neurons. However, for the practical case, more hidden neurons bring more interconnections, which require, in turn, larger training datasets for learning the relationships. It is therefore always necessary to optimize the number of neurons of the ANN hidden layers, as demonstrated by Demuth and Beale (2000).

5.2 Performance evaluation measures

It is very useful from the designer point of view to have an neural system aids to decide whether his suggested design is suitable or not by Compute the Mean Square error MSE from equation

$$MSE = \sum \left(\left(C_{ij} \right)_{nn} - C_{ij} \right)^2 / n \tag{7}$$

Where $\left(C_{ij} \right)_{\mathrm{nn}}$ is the predicted capacitance change, C_{ij} the capacitance change measured from FEM, and n is the number of FEM measured data values.

Thus, the performance index will either have one global minimum, depending on the characteristics of the input vectors. Local minimum is the minimum of a function over a limited range of input values. Local minimum is an unavoidable when the ANN is fitted. So a local minimum may be good or bad depending on how close the local minimum is to the global minimum and how low an MSE is required. In any case, the method applied to solve this problem and descent the local minimum with momentum. Momentum allows a network to respond not only to the local gradient, but also to recent trends in the error surface. Without momentum a network may get stuck in a shallow local minimum.

5.3 Feedforward neural networks (FFNN)

Feed-forward neural networks (FFNN) in general consist of a layer of input neurons, a layer of output neurons and one or more layers of hidden neurons (Skapura 1996). Neurons in each layer are interconnected fully to previous and next layer neurons with each interconnection have associated connection strength or weight. The activation function used in the hidden and output layers neurons is nonlinear, where as for the input layer no activation function is used since no

computation is involved in that layer. Information flows from one layer to the other layer in a feed-forward manner. Various functions are used to model the neuron activity such as liner transfer function (purelin(n)), Tan-Sigmoid transfer function (tansig(n)) or Radial Basis (Gaussian) transfer functions (radbas(n)).

The training process is terminated either when the Mean-Square-Error (MSE) between the observed data and the ANN outcomes for all elements in the training set has reached a pre-specified threshold or after the completion of a pre-specified number of learning epochs.

5.3.1 A feed-forward Neural Network (FFNN) Design for ECS to study the effect of pipeline environment temperature (θ)

A feed-forward NN is shown in Fig. 7. The NN configuration in this case was $\{9\ [10\ 2]_2 1\}$, with tan-sigmoid neurons for the first layer while the second layer has pure linear ones. FFNN is trained by measuring values of ρ, φ, θ to predict corrosion rates C_{ij}. In the first FFNN structure is applied for training the data of ECS at normal temperature ($\theta = 25℃$). Fig. 8 shows the training performance of suggested FFNN. Fig.9 represents the comparison between the FE data and the feed forward neural network FFNN predicted data (ECS capacitance change) at ($\theta = 25℃$) for electrode pairs $C_{1\text{-}2}$ and $C_{1\text{-}13}$. The results of this NN show much satisfactory predication quality for this case study. Fig. 10 shows the comparison between the FE data and the feed forward neural network FFNN expected data at($\theta = 25℃$) for electrode pairs $C_{1\text{-}7}$ and $C_{1\text{-}8}$. From this Figure, it noted that the expected data from the suggested FFNN are applicable with the FE data.

Table 2 gives the values of mean square error (MSE) (see Eq. (6)) between the expected and FE data for both FFNN predicted for electrode pairs $C_{1\text{-}2}$ and $C_{1\text{-}13}$ and FFNN expected data for electrode pairs $C_{1\text{-}7}$ and $C_{1\text{-}8}$, at($\theta = 25℃$), in order to obtain the best performances of the present network.

Table 2 Mean square error (MSE) values

$\boldsymbol{\theta = 25℃}$		
Data	**Electrode pairs**	**MSE**
Predicted	$\mathbf{C_{1\text{-}2}}$	7.6034 E-7
	$\mathbf{C_{1\text{-}13}}$	4.3213 E-6
Expected	$\mathbf{C_{1\text{-}7}}$	1.1835 E-5
	$\mathbf{C_{1\text{-}8}}$	2.0552 E-5

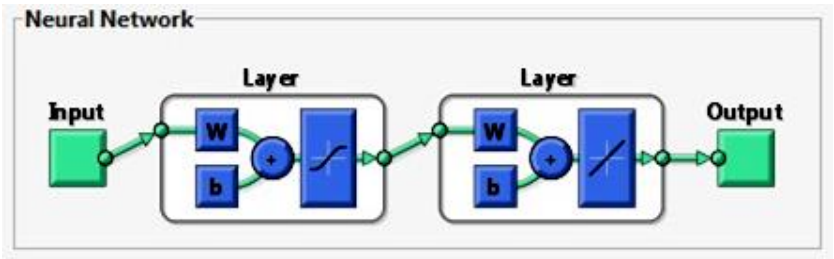

Fig. 7 Schematic illustration of FFNN design for present study with input data ρ, θ, φ

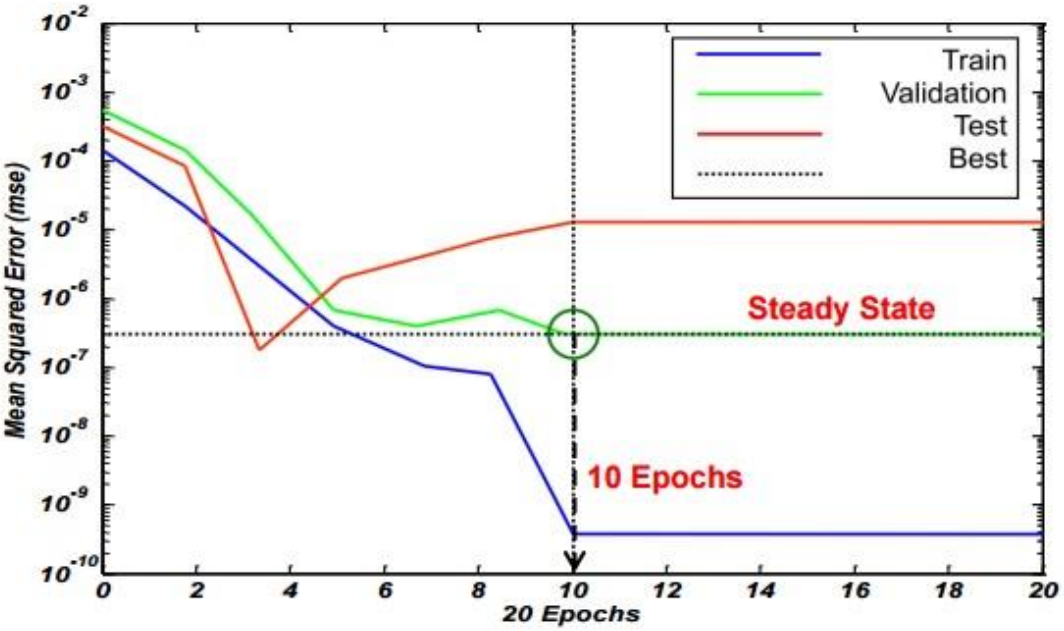

Fig. 8 Training performance of suggested FFNN

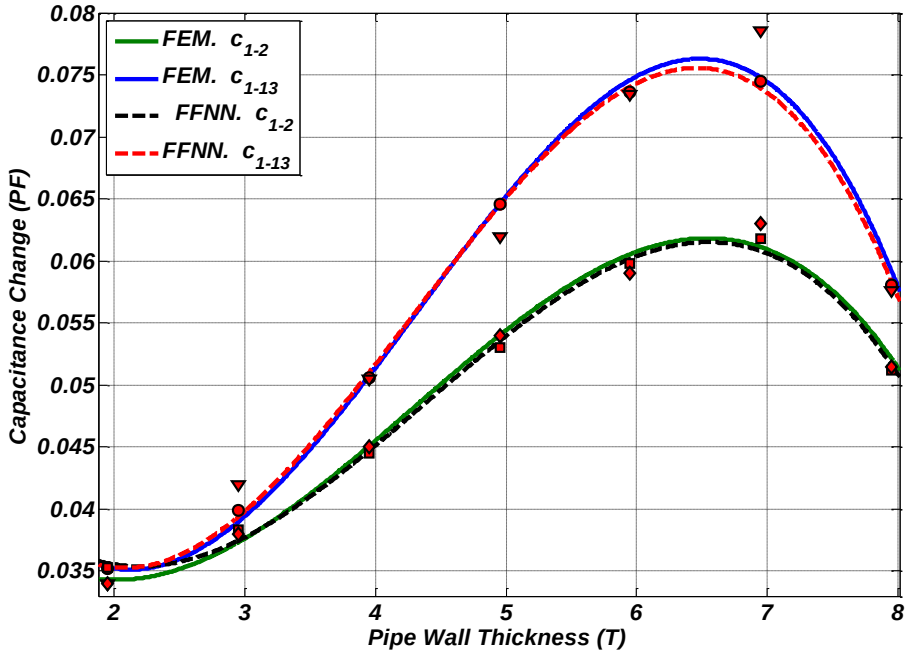

Fig. 9 Comparison between the FE data and FFNN predicted data for C_{1-2} and C_{1-13} at $\theta = 25℃$

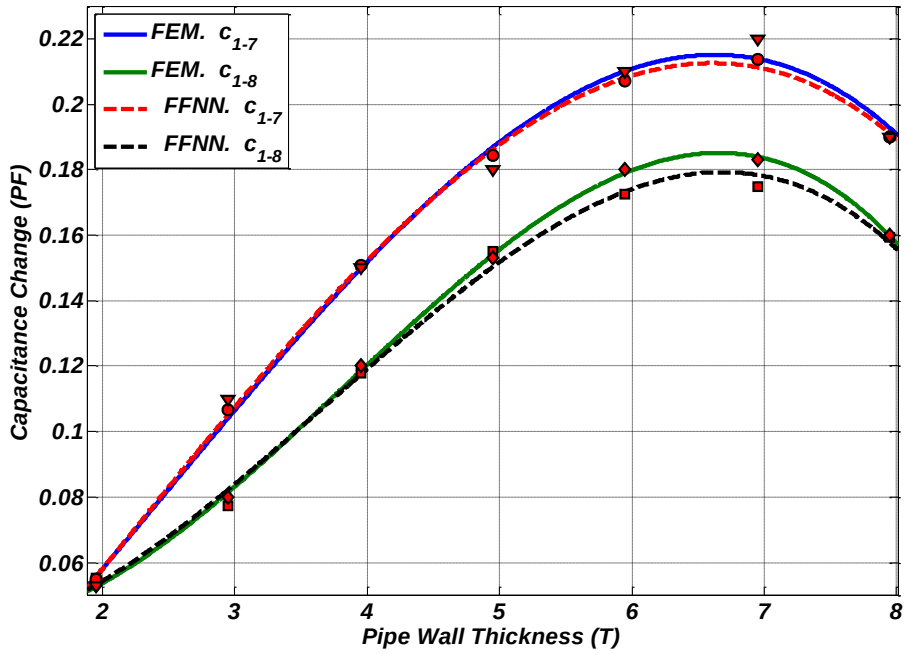

Fig. 10 Comparison between the FE data and FFNN Expected data for C_{1-7} and C1-8 at $\theta = 25℃$

5.4 The use of present FFNN in predicting non-FE data

The main goal of the artificial neural network design is predicting non-FE data. In this section we will use the suggested FFNN to predict some non-FE data not included in FE evaluation. It is selected to use three different values of pipeline environment temperature (θ) of 40℃, 60℃ and 80℃ and random values of pipe wall thickness (X) for all electrode pairs C_{ij}. The previous three parameters are the input vectors for artificial neural network, while the output is the signal vector; the corrosion rates.

Fig. 11 to Fig. 13 represent the pipe wall thickness (X) against the capacitance change output from artificial neural network for all pipeline environment temperature (θ) of 40℃, 60℃ and 80℃ respectevely. Using the exponential formula $C_{ij} = a_{ij}e^{b_{ij}X} + k_{ij}e^{h_{ij}X}$ have proved its suitability by giving acceptable values for the correlation factors (C.F) are very near to unity.

Comparing the result predicted from artificial neural network and data obtained from FE method for the other values of pipeline environment temperature (θ), Table 3 it is conclude that the present artificial neural network is suitable and useful in predicting non-FE data.

5.5 The effect of pipeline environment temperature (θ)

Analyzing the values of four constants (a_{ij}), (b_{ij}), (k_{ij}) and (h_{ij}) taking into account the variation of pipeline environment temperature (θ), capacitance change (C_{ij}), and pipeline thickness (X) or radius-electrode ratio (ρ), and considering Table 3 resulted in the following:

1) For all pipeline environment temperature (θ), at maximum points, the tendency curve of capacitance change against X for capacitance change (C_{1-3}) has the highest capacitance change, the tendency curve for capacitance change (C_{1-2}) has the lowest capacitance change, while the other curves for the remaining capacitance change laid in between, with descending order from (C_{1-4}) to (C_{1-13}).
2) The values of the constants (a_{ij} & k_{ij}) were found to depend on the pipeline environment temperature (θ) for capacitance change (C_{ij}), as the pipeline environment temperature (θ) increases the absolute value of (a_{ij} & k_{ij}) will decreases, i.e. the capacitance change increased, means the corrosion rates increased.
3) The deviation in the values of the constants (b_{ij} & h_{ij}) at all pipeline environment temperature (θ) is negligible and it may be considered constant, the average value (Avg.) of constants (b_{ij} & h_{ij}) was calculated and considered to be used at any temperature (θ), as the corresponding standard deviation (S.D) was found to have acceptable values, as shown in Table 3.

6. Conclusions

For this work, the finite element method (FEM) and artificial neural network (ANN) techniques were used for modeling and simulating the electrical capacitance sensor (ECS) sensor to detect the corrosion rates inside steel pipelines and study and predict the effect of pipeline environment temperature (θ) on the corrosion rates, the following conclusions can be drawn:

1) The pipeline internal corrosion is means decrease of the pipeline thickness was discussed completely by FEM numerical simulation software ANSYS. The influence of pipeline to electrode pairs decreases followed by (C_{1-3}, C_{1-4}, C_{1-5}, C_{1-6}, C_{1-7}, C_{1-8}, C_{1-9}, C_{1-10}, C_{1-11}, C_{1-12}, C_{1-13} and C_{1-2}). Maximum capacitance change is gotten at X = 6.95 mm, ρ = 0.79, which is beneficial for capacitance measurement. With the decrease of pipe wall thickness (X) or increase of the radius-electrode ratio (ρ), the distortion of ECS sensitivity becomes more serious.
2) An artificial neural network can be used as a method for simulating the ECS to expect the non-FE Data of capacitance change at the pipeline environment temperature $\theta = 25℃, 40℃, 60℃$ and $80℃$.
3) Training a neural network is heavily time consuming.
4) Using the exponential formula $C_{ij} = a_{ij}e^{b_{ij}X} + k_{ij}e^{h_{ij}X}$ has proved its suitability for present study, and it is found that, the deviation of the constants (b_{ij} & h_{ij}) for different pipeline environment temperature (θ) and capacitance change (C_{ij}) is negligible and it may be considered to be constant.
5) The value of the constants (a_{ij} & k_{ij}) were found to be depend on the pipeline environment temperature (θ) and the capacitance change (C_{ij}) with high correlation factors (C.F), as the pipeline environment temperature (θ) increases the value of (a_{ij} & k_{ij}) will decreases i.e. the pipeline environment temperature (θ) had a detrimental effect on the corrosion rates increases.
6) Finally, we can be concluded that the accuracy and reliability of the proposed technique are leads to better understanding of the corrosion mechanism under different pipeline environmental temperature.

Table 3 Corrosion rate Constants (a_{ij}), (b_{ij}), (k_{ij}) and (h_{ij}) at $\theta = 25℃, 40℃, 60℃$ and $80℃$

]	θ	C_{1-2}	C_{1-3}	C_{1-4}	C_{1-5}	C_{1-6}	C_{1-7}	C_{1-8}	C_{1-9}	C_{1-10}	C_{1-11}	C_{1-12}	C_{1-13}
a_{ij}	*25℃	-7867	-1107	-1533	-2860	-3277	-4094	-4718	-5964	-6254	-6823	-7072	-7643
	**40℃	-7713	-952	-1376	-2691	-3125	-3942	-4562	-5805	-6100	-6668	-6918	-7485
	**60℃	-7396	-632	-1054	-2372	-2806	-3623	-4241	-5493	-5785	-6353	-6593	-7173
	**80℃	-7172	-413	-832	-2158	-2581	-3411	-4028	-5272	-5552	-6126	-6372	-6951
$b_{ij} \times 10^{-4}$	*25℃	-0.1907	-0.1987	-0.1967	-0.1938	-0.1921	-0.1953	-0.1928	-0.1973	-0.1980	-0.1972	-0.1924	-0.1983
	**40℃	-0.1923	-0.1997	-0.1955	-0.1923	-0.1912	-0.1942	-0.1936	-0.1922	-0.1911	-0.1958	-0.1966	-0.1998
	**60℃	-0.1979	-0.1982	-0.1927	-0.1931	-0.1953	-0.1966	-0.1919	-0.1925	-0.1995	-0.1969	-0.1939	-0.1974
	**80℃	-0.1958	-0.1959	-0.1986	-0.1924	-0.1972	-0.1939	-0.1923	-0.1982	-0.1988	-0.1917	-0.1987	-0.1961
	Avg.	**-0.1942**	**-0.1981**	**-0.1959**	**-0.1929**	**-0.194**	**-0.195**	**-0.1926**	**-0.1951**	**-0.1969**	**-0.1954**	**-0.1954**	**-0.1979**
	S.D.	**0.0033**	**0.0016**	**0.0025**	**0.0007**	**0.0028**	**0.0012**	**0.0007**	**0.0031**	**0.0039**	**0.0025**	**0.0028**	**0.0016**
k_{ij}	*25℃	7867	1107	1533	2860	3277	4094	4718	5964	6254	6823	7072	7643
	**40℃	7713	952	1376	2691	3125	3942	4562	5805	6100	6668	6918	7485
	**60℃	7396	632	1054	2372	2806	3623	4241	5493	5785	6353	6593	7173
	**80℃	7172	413	832	2158	2581	3411	4028	5272	5552	6126	6372	6951
$h_{ij} \times 10^{-4}$	*25℃	0.1921	0.1986	0.1977	0.1927	0.1960	0.1964	0.1976	0.1978	0.1903	0.1929	0.1995	0.1973
	**40℃	0.1956	0.1945	0.1945	0.1941	0.1921	0.1949	0.1932	0.1998	0.1982	0.1941	0.1925	0.1946
	**60℃	0.1962	0.1969	0.1987	0.1911	0.1982	0.1962	0.1925	0.1999	0.1913	0.1964	0.1987	0.1997
	**80℃	0.1933	0.1948	0.1964	0.1987	0.1949	0.1942	0.1928	0.1983	0.1920	0.1981	0.1922	0.1921
	Avg.	**0.1943**	**0.1962**	**0.1968**	**0.1942**	**0.1953**	**0.1954**	**0.194**	**0.199**	**0.193**	**0.1954**	**0.1957**	**0.1959**
	S.D.	**0.0019**	**0.0019**	**0.0018**	**0.0033**	**0.0025**	**0.0011**	**0.0024**	**0.0011**	**0.0036**	**0.0023**	**0.0039**	**0.0033**
C.F	*25℃	0.9945	0.9921	0.9908	0.9369	0.9928	0.9701	0.9828	0.9628	0.9043	0.9946	0.9715	0.9932
	**40℃	0.9994	0.9995	0.9976	0.9921	0.9948	0.9999	0.9989	0.9983	0.9855	0.9993	0.9911	0.9897
	**60℃	0.998	0.9994	0.9946	0.9939	0.9991	0.9999	0.9921	0.9987	0.9963	0.9994	0.9993	0.9903
	**80℃	0.9977	0.9992	0.9973	0.999	0.9993	0.9999	0.9988	0.9991	0.9984	0.9993	0.9955	0.9999

*** FEM Data**
**** FFNN Expected Data**

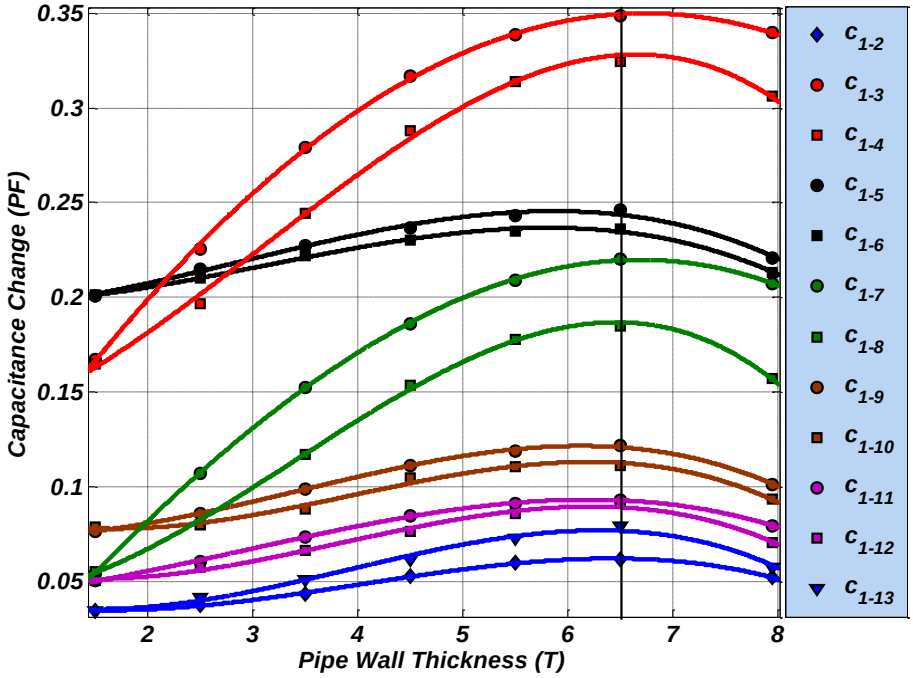

Fig. 11 Expected Data of Capacitance change at $\theta = 40℃$

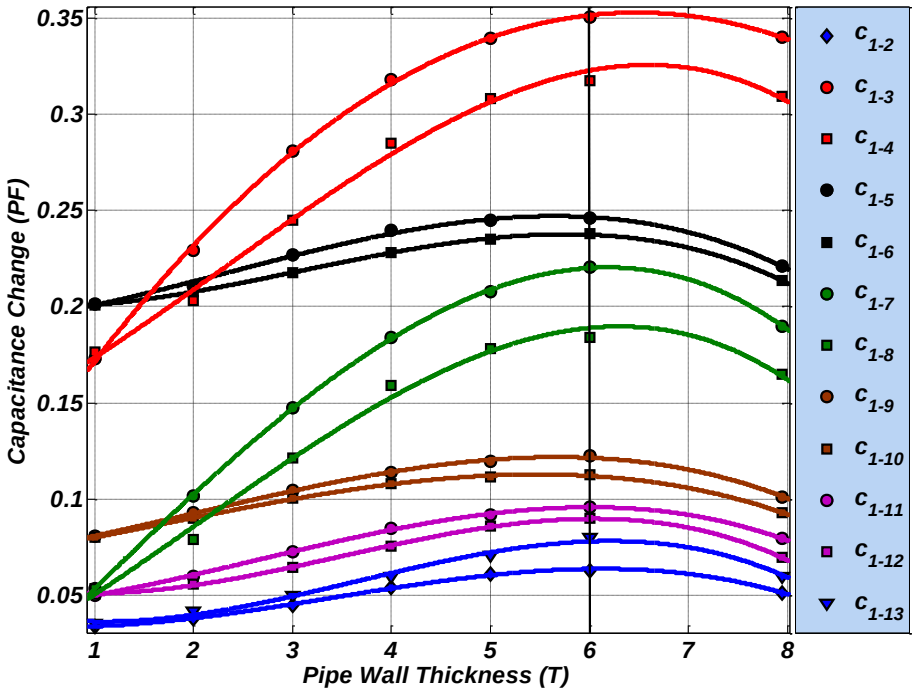

Fig. 12 Expected Data of Capacitance change at $\theta = 60℃$

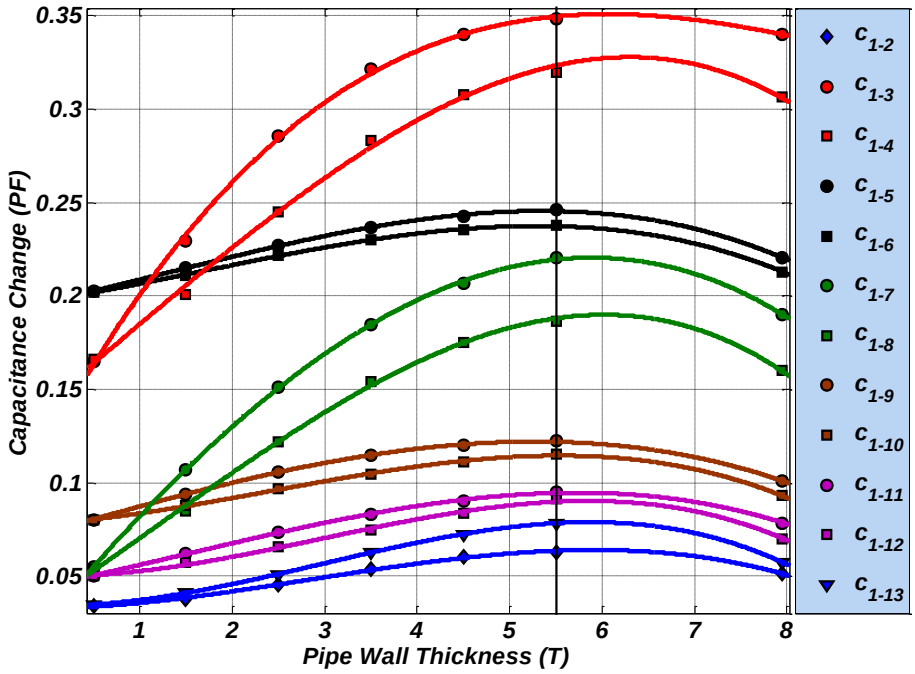

Fig. 13 Expected Data of Capacitance change at $\theta = 80℃$

References

Al-Tabey, W.A. (2010), "Effect of pipeline filling material on electrical capacitance tomography", *Proceedings of the International Postgraduate Conference on Engineering (IPCE 2010)*, Perlis, Malaysia, October 16-17.

Al-Tabey, W.A. (2012), "Finite Element Analysis in Mechanical Design Using ANSYS: Finite Element Analysis (FEA) Hand Book For Mechanical Engineers With ANSYS Tutorials", LAP Lambert Academic Publishing, Germany, ISBN 978-3-8454-0479-0.

Alwis, L., Sun, T. and Grattan, K.T.V. (2013), "Optical fibre-based sensor technology for humidity and moisture measurement: Review of recent progress", *Measurement*, **46**(10), 4052-4074.

ANSYS Low-Frequency Electromagnetic analysis Guide, The Electrostatic Module in the Electromagnetic subsection of ANSYS (2014), ANSYS, inc. Southpointe 275 Technology Drive Canonsburg, PA 15317, Published in the USA.

Cole, I.S. and Marney, D. (2012), "The science of pipe corrosion: A review of the literature on the corrosion of ferrous metals in soils", *Corros. Sci*., **56**, 5-16.

Daoye, Y., Bin, Z., Chuanlong, X., Guanghua, T. and Shimin, W. (2009), "Effect of pipeline thickness on electrical capacitance tomography", *Proceedings of the 6th International Symposium on Measurement Techniques for Multiphase Flows*, Journal of Physics: Conference Series **147**, 1-13.

Demuth H. and Beale M. (2000), "Neural Network Toolbox User's Guide for use with MATLAB Version 4.0", The Math Works, Inc.

Dong, S., Liao, Y. and Tian, Q. (2005a), "Intensity-based optical fiber sensor for monitoring corrosion of aluminum alloys", *Appl. Optics*., **44**(27), 5773-5777.

Dong, S., Liao, Y. and Tian, Q. (2005b), "Sensing of corrosion on aluminum surfaces by use of metallic optical fiber", *Appl. Optics*, **44**(30), 6334-6337.

Dong, S., Peng, P. and Luo, Y. (2007), "Preparation techniques of metal clad fibres for corrosion monitoring of steel materials", *Smart Mater. Struct*., **16**, 733-738.

Fasching, G.E. and Smith, N.S. (1988), "High Resolution Capacitance Imaging System", US Dept. Energy, **37**, DOE/METC-88/4083

Fasching, G.E. and Smith, N.S. (1991), "A capacitive system for 3-dimensional imaging of fluidized-beds", *Review of Scientific Instruments*, **62**, 2243-2251

He, Y. (2015), "Corrosion Monitoring", Reference Module in Materials Science and Materials Engineering, Science Direct.

Jaworski, A.J. and Bolton, G.T. (2000), "The design of an electrical capacitance tomography sensor for use with media of high dielectric permittivity", *Measurement Science and Technology*, **11**(6), 743-757.

Li, H. and Huang, Z. (2000), "Special measurement technology and application", Zhejiang University Press, Hangzhou.

Li, X.M., Chen, W., Zhu, Y., Huang, S. and Bennett, K.D. (2000), "Monitoring the corrosion of steel in reinforced concrete using optical waveguide methods", *Smart Struct. Mater*., 2000: Sensory Phenomena and Measurement Instrumentation for Smart Structures and Materials, **3986**, 172-179.

Pei, T. and Wang, W. (2009), "Simulation analysis of sensitivity for electrical capacitance tomography", *Proceedings of the 9th International Conference on Electronic Measurement & Instruments (ICEMI 2009)*.

Sinchenko, E. (2013), "Fiber optical distributed corrosion sensor", Ph.D. Dissertation, Faculty of Engineering and Industrial science Swinburne University of Technology, Melbourne, Australia.

Skapura, D. (1996), "Building Neural Networks", ACM Press, Addison-Wesley Publishing Company, New York.

Xie, C.G., Huang, S.M., Hoyle, B.S., Thorn, R., Lenn, C., Snowden, D. and Beck, M.S. (1992), "Electrical capacitance tomography for flow imaging: system model for development of image reconstruction algorithms and design of primary sensors", *IEEE Proceedings-G*, **139**(1), 89-98.

Yang, W.Q. (1997), "Modelling of capacitance sensor", *IEEE proceedings: Measurement Science and Technology*, **144**(5), 203-208.
Yang, W.Q. and York, T.A. (1999), "New AC-based capacitance tomography system", *IEEE proceedings: Measurement Science and Technology*, **146**(1), 47-53.
Yang, W.Q., Beck, M.S. and Byars, M. (1995b), "Electrical capacitance tomography–from design to applications", Measurement & Control, **28**(9), 261-266
Yang, W.Q., Stott, A.L., Beck, M.S. and Xie, C.G. (1995a), "Development of capacitance tomographic imaging systems for oil pipeline measurements", *Review of Scientific Instruments*, **66**(8), 4326

HL